Astron. Astrophys. 327, 1230–1241 (1997)

ASTRONOMY
AND
ASTROPHYSICS

Simultaneous temperature and density diagnostics of optically thin plasmas

E. Landi and M. Landini

Department of Astronomy and Space Science, University of Florence, Italy

Received 12 December 1996 / Accepted 26 May 1997

Abstract. A method is given for performing simultaneous temperature and density diagnostics of an optically thin plasma by means of all the available observations of lines of the same ions. The density and differential emission measure at selected temperatures may be measured and the chemical composition verified. The method is applied to line emission measured by SERTS 89 for an active region of the solar corona and use is made of the Arcetri spectral code and the CHIANTI atomic data base to evaluate the theoretical expected intensities. Lines of He II, C IV, Ne V and VI, Mg VI,VII,VIII and IX, Si VIII,IX,X and XI, S XIII and XIV, Cr XIII and XIV, Fe X,XI,XII,XIII XIV,XV,XVI and XVII and Ni XVIII are used to put constraints on the model of the density versus temperature and on the Differential Emission Measure, and suggestions are given on how to use the method to verify intensity calibrations and identify lines for which atomic physics must be improved.

Key words: atomic data – plasmas – Sun: corona – Sun: X-rays

1. Introduction

The electron density and temperature are fundamental pieces of information needed to understand the physics of both cosmic and laboratory plasmas. In particular the study of the outer atmospheres of the Sun and the active stars requires the knowledge of density and temperature to model very different structures such as coronal holes, active loops, flares, and to evaluate radiative losses, a fundamental component of the energy budget, necessary to investigate the problem of coronal heating.

The soft x-ray and extreme ultraviolet region of solar and stellar spectra contain many bound-bound transitions of ions formed over a wide range of temperature and density regimes, and the line emission in this spectral region is an excellent tool to determine the physical conditions of the plasma.

While the temperature distribution of matter within the source is investigated by comparing the absolute intensity of a number of lines of ions formed in many very different temperature conditions, the most commonly used technique for measuring the electron density concerns the ratio of proper line pairs which originates from upper levels of the same ions with different density dependent populations. This technique has been extensively used to measure electron density in flares, active and quiet regions of the transition region and the corona of the Sun and the stars by means of soft x-rays and extreme ultraviolet lines. Comparison between the estimated density and the Emission Measure allows to evaluate the "true" volume of the source and to find whether the emitting volume completely fills the single pixels of the image, or filamentary structure is present.

Detailed and careful reviews of this method and of the most important results are available (Doschek 1990; Mason 1991; Dwivedi 1994).

However the line pairs ratio method assumes that the source of the two lines is strictly isothermal and the measured density is usually assigned to the region where the temperature equals the temperature of maximum abundance of the ion.

This is completely arbitrary and the simultaneous presence of spectral lines of very different ion stages is clear evidence of the contribution of different temperature regions along the line of sight. The *Differential Emission Measure (d.e.m.)* has been introduced to take into account the non isothermal nature of the radiation source in the solar corona and has proved to be very suitable for describing any type of source from coronal holes to flares.

The aim of this paper is to describe a improved method for evaluating the mean electron density of the region where the line is formed, without the isothermal hypothesis and using a proper definition of the effective temperature associated with the line radiation. Furthermore, no line pairs ratio are necessary since each line is considered independently. This helps to identify the "wrong" lines in the common situation when not all the lines of the same ion fit the same density solutions. Moreover, this method also allows the d.e.m. of the emitting region, to be evaluated.

In Sect. 2 the method is described and the procedures to evaluate density and d.e.m. are discussed. In Sect. 3 the method

Send offprint requests to: E. Landi

is applied to SERTS 89 observations, the data analysis is performed, and a detailed discussion of the results for many ions is given.

2. The theoretical method

2.1. The plasma emissivity

The number of photons emitted in a bound-bound transition from upper level *j* to lower level *i* per unit volume and time is

$$\varepsilon_{ij} = N_j(X^{+m})A_{ij} \qquad \text{ph cm}^{-3}\text{s}^{-1} \tag{1}$$

where $N_j(X^{+m})$ is the population of the level j of the ion of charge $+m$ of element X and A_{ij} the spontaneous radiative transition probability of the $j-i$ transition.

It is usual to write

$$N_j(X^{+m}) = \frac{N_j(X^{+m})}{N(X^{+m})}\ \frac{N(X^{+m})}{N(X)}\ \frac{N(X)}{N(H)}\ \frac{N(H)}{N_e}\ N_e \tag{2}$$

where $\frac{N_j(X^{+m})}{N(X^{+m})}$ describes the population of level j relative to the total ion, $\frac{N(X^{+m})}{N(X)}$ is the relative abundance of the ion X^{+m} assuming ionization equilibrium, $\frac{N(X)}{N(H)}$ is the abundance of the X element relative to Hydrogen and $\frac{N(H)}{N_e}$ is about 0.8 in a completely ionized plasma of cosmic composition.

The number of photons that we receive at distance *d* from each pixel of the image covering an area *S*, is the contribution along the line of sight *h*

$$P_{ij} = \frac{1}{4\pi}\ \int_h N_j(X^{+m})A_{ij}\frac{S}{d^2}dh \tag{3}$$

Because $\frac{S}{d^2}$ is the solid angle covered by the pixel the intensity is

$$I_{ij} = \frac{1}{4\pi}\ \int_h N_j(X^{+m})A_{ij}dh \quad \text{ph cm}^{-2}\ \text{s}^{-1}\ \text{sterad}^{-1} \tag{4}$$

We can define the $Contribution\ Function$ as follows:

$$G_{ij}(T,N_e) = \frac{N_j(X^{+m})}{N(X^{+m})}\ \frac{N(X^{+m})}{N(X)}\ \frac{N(X)}{N(H)}\ \frac{N(H)}{N_e}\ \frac{A_{ij}}{N_e} \tag{5}$$

For resonance lines in very low density limit

$$N_j(X^{+m})\ A_{gj} = N_g(X^{+m})N_eC_{g,j} \simeq N(X^{+m})N_eC_{g,j} \tag{6}$$

the $Contribution\ Function$ reduces to the usual form

$$G_{gj}(T) = \frac{N(X^{+m})}{N(X)}\ \frac{N(X)}{N(H)}\ \frac{N(H)}{N_e}\ C_{gj} \tag{7}$$

and the line intensity is

$$I_{gj} = \frac{1}{4\ \pi}\ \int_h G_{gj}(T)N_e^2dh \tag{8}$$

To evaluate the $Contribution\ Function$ use have been done of some recent ionization equilibrium computations (Arnaud and Rothenflug 1985, Arnaud and Raymond 1992). They do not include density dependent processes, which are expected to affect only dielectronic recombination for rather high density (Jordan 1969).

When forbidden or intercombination lines are considered, the population of all the relevant levels must be computed assuming statistical balance among the most important processes, mainly electron collisional excitation and decay and radiative decay. In this case $\frac{N_j(X^{+m})}{N(X^{+m})}$ may depend remarkably on density and very smoothly on temperature.

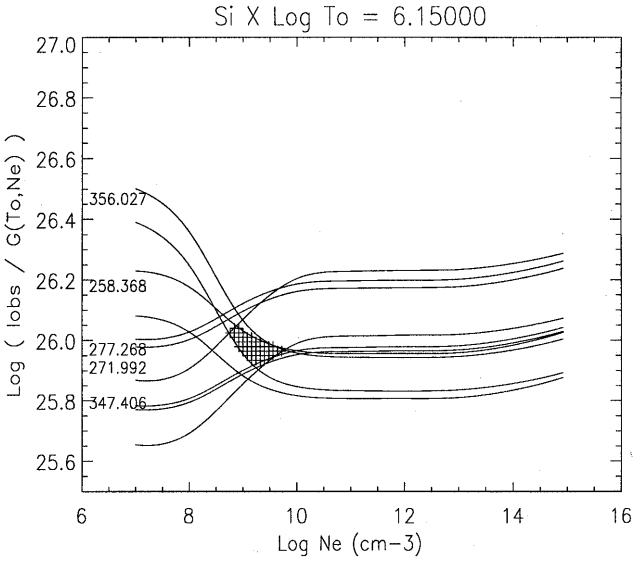

Fig. 1. The ratio of the observed intensity to the $G(N_e, T_o)$ is plotted versus the logarithmic density for all the lines of Si X. For each line the observed intensity plus and minus the error is considered.

2.2. The diagnostic technique

The suggested diagnostic is performed in a very simple way: the ratio of the measured intensity of each line of a selected ion, over the emissivity $G_{ij}(T_o, N_e)$ at a proper temperature T_o is plotted versus $logN_e$. All the ratios meet within a restricted region of the diagram depending on the errors as shown for instance in Fig.1.

This example is obtained using five lines of SiX measured by SERTS89 and given in erg cm^{-2} s^{-1} sterad^{-1} and evaluating the $G_{ij}(T, N_e)$, in erg cm^3 s^{-1}, for each line with the CHIANTI database. The coordinates of the meeting point are the density at T_o and the weighted emission measure for temperature T_o, (see eq 18).

A better example is given by the simulation of Fig. 2 where the synthetic flux is evaluated for seven lines of FeXIII using a sharp dem and electron density 10^9 cm^{-3} and used as "observed intensity" in the plot.

In this case, when "observed data" are simulated and no error is added, all the curves cross the same point at the density used for the simulation.

In the following of this section, we will show:

- the reason why all the curves meet at the same density, when no strong inhomogeneity occurs along the line of sight
- how the ordinate of of the crossing point is related to the d.e.m.
- how to evaluate the proper temperature T_o

Basically this method rests on the observation that the dependence of the $ContributionFunction$ on N$_e$ and T is such that we can express $G_{ij}(T, N_e)$ as the product of two distinct

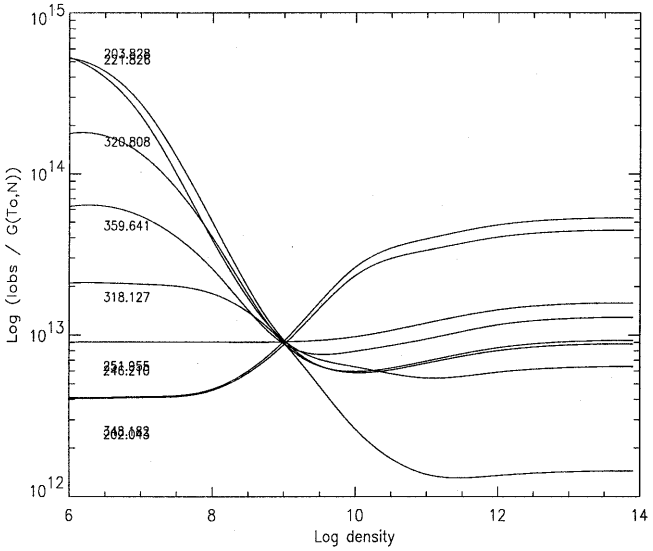

Fig. 2. The synthetic flux of several Fe XIII lines evaluated for density $N_e = 10^9$ is used to show that all the lines cross at the correct density

functions depending respectively on electron density and electron temperature, and on temperature alone:

$$G_{ij}(T, N_e) = f_{ij}(N_e, T)\ g(T) \tag{9}$$

The variation of the $g(T)$ functions is mainly due to the ionization equilibrium and is the same for all the lines of the same ion while $f(N_e, T)$ is determined mainly by the population of the upper level. The dependence of G_{ij} on electron density is mainly due to the collisional population and depopulation processes determining the statistical equilibrium term $\frac{N_j(X^{+m})}{N(X^{+m})}$ of the upper atomic level j. The dependence of G_{ij} on temperature comes both from the ionization equilibrium term $\frac{N(X^{+m})}{N(X)}$ for the ion X^{+m} and from the population of the upper atomic level j.

Fig. 3 elucidates the above considerations; as an example, the emissivity of FeXIII 318.127 Å for different densities is divided by the G(T) function of FeXIII 251.95 Å, in order to remove the common temperature dependence g(T); this line is very weakly density sensitive and its G(T) has been evaluated at $N_e = 10^{10}$. The electron density (cm^{-3}) labels each curve. Clearly the $f(N_e, T)$ of line 318.127 is strongly density dependent between 10^9 and 10^{11} and very weakly dependent on temperature for any density. A straight line fits each curve within a few percent. This property holds quite usually and in any case may be easily verified before the method is applied. When comparison is made with observations, such as in Sect. 3, this procedure has been applied to all the lines of the same ion, assuming as g(T) for each ion, the G(T) of the less density sensitive line.

In order to take into account the non isothermal nature of the plasma along the line of sight, as usual, the $d.e.m.$ is introduced

$$d.e.m. = \varphi(T) = N_e^2 \frac{dh}{d\ T} \tag{10}$$

and the intensity of a line can be rewritten

$$I_{ij} = \frac{1}{4\ \pi} \int_h G_{ij}(T, N_e) N_e^2 dh =$$

$$= \tfrac{1}{4\ \pi} \int_T f_{ij}(T, N_e) g(T) \varphi(T) dT \tag{11}$$

Since $f(N_e, T)$ is nearly a linear function of Log$T$ for all the temperatures of interest in a stellar corona, we can expand the $f(N_e, T)$ function as a power series of Log T around the point Log T_o and consider only the first term of this expansion.

$$f_{ij}(N_e, T) = f_{ij}(N_e, T_o) + \left(\frac{\partial f}{\partial LogT}\right)_{T_o} (LogT - LogT_o) +$$

$$+ O\big((LogT - LogT_o)^2\big) \tag{12}$$

The $\varphi(T)$ function is not known but if a "trial" d.e.m. $\varphi_t(T)$ is known, (see next section) the "true" $\varphi(T)$ may be written

$$\varphi(T) = \varepsilon(T)\ \varphi_t(T) \tag{13}$$

If $\varphi_t(T)$ is a reasonable approximation to $\varphi(T)$, $\varepsilon(T)$ is likely to be a slow function of T very near to 1 and may be put as

$$\varepsilon(T) = \varepsilon(T_o) + \left(\frac{\partial \varepsilon}{\partial LogT}\right)_{T_o} (LogT - LogT_o) +$$

$$+ O\big((LogT - LogT_o)^2\big) \tag{14}$$

If the temperature region where the line is formed is not inhomogeneous , one may assume that only one mean electron density $N_e^\star$ occurs and neglecting contributions of second order, the previous equations allow the observed intensity to be expressed as a sum of two distinct contributions:

$$I_{ij} = \frac{1}{4\ \pi}\left[f_{ij}\big(N_e^\star, T_o\big)\ \varepsilon(T_o) \int g(T)\ \varphi_t(T)\ dT \right] +$$

$$+ \frac{1}{4\ \pi}\left[\left(f_{ij}\big(N_e^\star, T_e^o\big) \frac{\partial \varepsilon}{\partial LogT} + \varepsilon(T_o) \frac{\partial f}{\partial LogT} \right) \right] \times$$

$$\times \int g(T)\ \ \varphi_t(T)(LogT - LogT_o)\ dT \tag{15}$$

where $N_e^\star$ represents the electron density of the emitting plasma. If we choose the temperature T_o as

$$LogT_o = \frac{\int g(T)\ \varphi_t(T)\ logT\ dT}{\int g(T)\ \varphi_t(T)\ dT} \tag{16}$$

the contribution from the linear term $(LogT - LogT_o)$ vanishes and the expression reduces to

$$I_{ij} = \tfrac{1}{4\ \pi}\ f_{ij}\big(N_e^\star, T_o\big) \varepsilon(T_o) \int g(T)\ \varphi_t(T)\ dT \tag{17}$$

It is very important to note that in this final equation the dependence of I_{ij} on the electron density N_e is separated from the dependence on the electron temperature T.

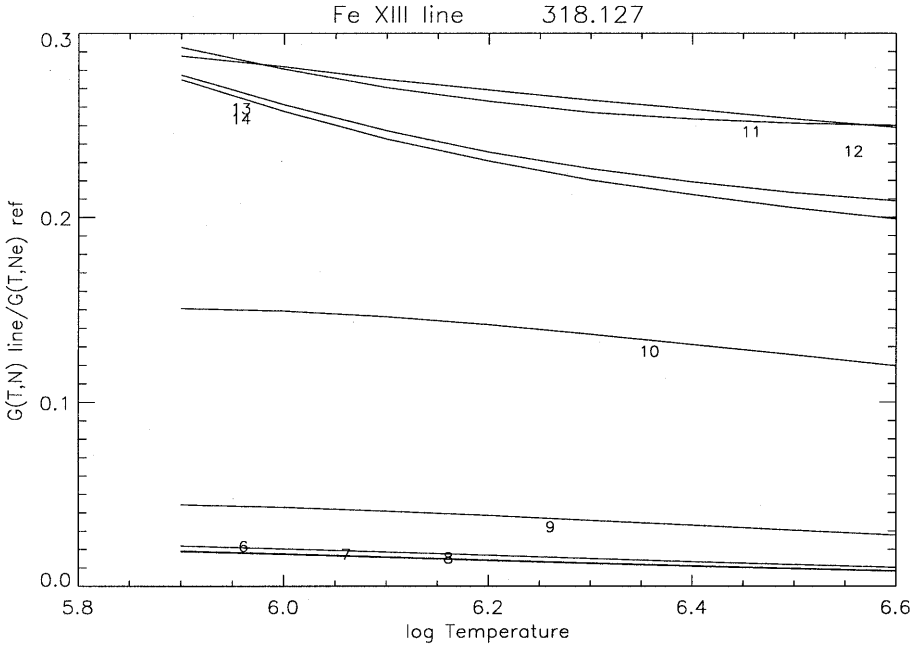

Fig. 3. Emissivity functions for line 318.127 Å of Fe XIII referred to line 251.950 Å of the same ion for electron density $N_e = 10^{10}$ cm^{-3} ; each curve is labeled with log of electron density; a straight line fits each curve to within a few percent

This property allows to define the function $L_{ij}(N_e)$ as the ratio between the observed line intensity and the $ContributionFunction\ G_{ij}(T_o, N_e)$ calculated as a function of N_e at the temperature T_o:

$$L_{ij}(N_e) = \frac{I_{obs}}{G_{ij}(T_o, N_e)} =$$

$$= \frac{1}{4\pi}\ \frac{f_{ij}(N_e^\star, T_o)}{f_{ij}(N_e, T_o)} \varepsilon(T_o)\ \int\ \frac{g(T)}{g(T_o)}\ \varphi_t(T)\ dT \qquad (18)$$

We note that the integral gives the same result for *all* the spectral line belonging to the same ion X^{+m} since $g(T_o)$ is the same for any line of the same ion. Thus, for all the spectral lines of the same ion the $L_{ij}(N_e)$ function can be reduced to the form

$$L_{ij}(N_e) = K'\ \frac{f(N_e^\star)}{f(N_e)} \qquad (19)$$

where

$$K' = \frac{1}{4\pi}\ \varepsilon(T_o)\ \int\ \frac{g(T)}{g(T_o)}\ \varphi_t(T)\ dT \qquad (20)$$

When $N_e = N_e^\star$ the ratio $\frac{f(N_e^\star)}{f(N_e)}$ becomes equal to 1 and the L_{ij} function has the value

$$L_{ij}\left(N_e^\star\right) = K' \qquad (21)$$

the same for all the lines of the same ion.

The measured K' allows $\varepsilon(T_o)$ to be evaluated , to obtain a better approximation of $\varphi(T)$ and start an iterative procedure, if the values of $\varepsilon(T_o)$ are significantly different from 1.

In this way when the $L_{ij}(N_e)$ functions of an ion are plotted versus density in the same diagram, all the curves meet in the same point $\left(N_e^\star, L_{ij}\left(N_e^\star\right)\right)$ if a mean electron density exists over the temperature region where the ion is formed. The value of the abscissa at the crossing point $N_e^\star$ is the value of the electron density that fits all the observations and can be taken as the value of the electron density at T_o.

This density diagnostic method is still suitable in the case that the observed intensity I_{obs} is given by the sum of the contributions of n_{lines} unresolved spectral lines belonging to the same ion. In this case we can define a new $L_{ij}(N_e)$ function as follows:

$$L_{ij}(N_e) = \frac{I_{obs}}{\Sigma_{i=1}^{n_{lines}}\ G_i(N_e, T)} \qquad (22)$$

Since all the lines belong to the same ion, the temperature sensitive part of the $ContributionFunction\ g(T)$ is the same for all spectral lines. Using the same approximations for the function $f(N_e, T)$ we obtain

$$L_{ij}(N_e) = \frac{1}{4\pi}\ \frac{\Sigma_{i=1}^{n_{lines}}\ f_i\left(N_e^\star, T_o\right)}{\Sigma_{i=1}^{n_{lines}}\ f_i(N_e, T_o)}\ \int\ \frac{g(T)}{g(T_o)}\varphi(T)\ dT$$

$$L_{ij}(N_e) = K'\ \frac{\Sigma_{i=1}^{n_{lines}}\ f_i(N_e^\star)}{\Sigma_{i=1}^{n_{lines}}\ f_i(N_e)} \qquad (23)$$

Again, a plot of the new $L_{ij}(N_e)$ versus the electron density will show that for $N_e = N_e^\star$ the curve will meet the same point $\left(N_e^\star, K'\right)$ as any other fully resolved transition of the spectrum of the ion X^{+m}.

It is worth underlining some properties of the L function:

- Density insensitive lines must have identical L functions within the experimental uncertainties.
- Lines that depend on the electron density in the same way must have identical L functions within the experimental uncertainties.
- Lines originated from the same upper level must have identical L functions.

2.3. The differential emission measure evaluation

The only problem of the density diagnostic method lies in the calculation of the temperature T_o, since its definition involves a "trial" $d.e.m.$ of the emitting source. In literature several different methods for calculating the $d.e.m.$ have been developed, using different algorithms and approximations; a comprehensive description of the most important ones and a critical assessment and comparison of their reliability can be found in Harrison and Thompson (1992).

In this paper we present a new method to evaluate the d.e.m. which adopts the same iterative procedure described in the previous section and uses density independent lines.

We assume that a trial d.e.m. $\varphi_o(T)$ is known; using a *Correction Function* $\omega(T)$, the true $\varphi(T)$ is

$$\varphi(T) = \omega(T)\ \varphi_o(T) \tag{24}$$

as before

$$\omega(T) = \omega(T_t) + \frac{\partial \omega}{\partial\ LogT}\ (LogT - LogT_t) + $$

$$+ O\left((LogT - LogT_t)^2\right) \tag{25}$$

The intensity of the emitted line then can be expressed as

$$I_{ij} = \frac{1}{4\ \pi}\left[\ \omega(T_t)\ \int\ G_{ij}(T)\ \varphi_o(T)\ dT\right] + \frac{1}{4\ \pi}\left(\frac{\partial \omega}{\partial LogT}\right)_{T_t} \times$$

$$\times \int\ (LogT - LogT_t)\ G_{ij}(T)\ \varphi_o(T)\ dT \tag{26}$$

If we define the temperature T_t as

$$LogT_t = \frac{\int G_{ij}(T)\ \varphi_o(T)\ logT\ dT}{\int G_{ij}(T)\ \varphi_o(T)\ dT} \tag{27}$$

then the contribution of the linear term to the total intensity of a density independent line vanishes and we can express the total observed intensity I_{ij} for the transition as

$$I_{ij} = \frac{1}{4\pi}\ \omega(T_t)\ \int\ G_{ij}(T)\ \varphi_o(T)\ dT \tag{28}$$

from which the correction $\omega(T_t)$ for each line may be computed and the first approximation $\varphi(T_t)$ evaluated. A spline function is drawn through the $\varphi(T_t)$ and the procedure is repeated until the $\omega(T)$ are all equal to 1 within the errors, or the best χ^2 is reached.

The procedure for d.e.m. evaluation proved to be very quick since only few steps are required in order to reach the condition of constant Correction Function. The convergence of the results to the true d.e.m. has been checked extensively using simulated observed intensities.

As usual for diagnostic procedures, a lot of information may be obtained by the analysis of $\omega(T)$ for differnt lines; disagreement among $\omega(T)$ values for lines of the same ion, may suggest problems of atomic physics, blending with other lines, inadequate calibrations. Systematic disagreement of $\omega(T)$ values for different ions of the same element may be used to check the ionization balance; systematic disagreement of $\omega(T)$ values belonging to ions of different elements may allow the chemical composition to be verified.

2.4. Discussion

This method is particularly suitable when high resolution spectra, such as those provided by SERTS or CDS and SUMER spectrographs on SOHO, are available and several lines of the same ions may be observed simultaneously. Nevertheless very accurate radiative and collisional transition probabilities are necessary since these data are essential for the calculation of the $ContributionFunction$ for each transition. The quality of the theoretical data adopted for the calculation of the theoretical $G(T, N_e)$ functions is very critical because it affects the analysis of the observed spectrum and the measurements of the electron density. In the present work we have made use of the Arcetri spectral code updated with the CHIANTI database (Dere et al. 1996). This databank is very extended and includes very carefully assessed atomic data both of radiative transition probabilities and electron-ion collision strengths.

The main advantage for the use of this method lies in the fact that it makes possible to study directly the behavior of each line of the spectrum comparing it with the behavior of all the other lines of the same ion. In a single plot all the informations concerning density sensitive and insensitive lines of the same ion may be shown. All the curves meet in a narrow range of values around the point $\left(N_e^\star, L\left(N_e^\star\right)\right)$ and a measure of the mean electron density of the emitting plasma is provided.This method is more convenient than the traditional line pairs ratio and the problem to find different solutions of the measured $N_e^\star$ using different line pairs is then overcome. Lines not sharing the common meeting point are immediately identified.

As for the d.e.m. analysis ,but in a more complete way, they may suggest either misidentifications, or blendings, or inaccurate atomic physics. Systematic effects are easily recognized and must be accurately investigated; disagreements common to the same range of wavelength may indicate calibration problems; disparities common to ions of the same element point to chemical composition; discrepancies occurring for consecutive ions show that the ionization balance may be questionable.

3. The Serts 89 spectrum

3.1. The data

The diagnostic method shown in Sect. 2 is applied to the solar spectrum observed with the Solar Euv Rocket Telescope and Spectrograph (S.E.R.T.S.) during the flight of May, 5 1989 (Thomas and Neupert 1994). During the flight an active region was observed by the telescope and a small rising subflare happened to be included in the field of view of the instrument.

The authors kindly supplied the averaged intensities for the lines, both for the Subflare and the Active Region component.

The data are provided in Tables 2 and 3 where only the lines used in the following analysis are included. No lines identified in the 1994 paper as a blend were included in the line list. In the present paper only the Active Region intensities are considered.

The theoretical data adopted for this study come from the CHIANTI database (Dere et al. 1996), and have been used to calculate the $ContributionFunctions$ assuming Feldman chemical composition (Feldman et al. 1992). Since measured intensities are in ergs instead of photons, $ContributionFunctions$ defined in eq 5 have been multiplied for the photon energy.

The complete set of data for the active region has been analyzed and the results are discussed in detail in the following sections.

3.2. Differential emission measure analysis

Following the procedure described in Sect. 2.3 we have used all the density insensitive lines available to derive the d.e.m. of the emitting source. The selected lines are reported in table 1.

The resulting d.e.m. is provided in Fig. 4 as a function of electron temperature.

Ten lines (starred in the table) have been excluded for the following reasons that clearly become apparent during the d.e.m. procedure:

- Mg V line at 353.08 is weaker than expected and does not agree with the other Mg V line.
- Ne VI lines at 433.16 Å and 435.63 Å , Mg VIII lines at 430.44 Å ,and also 436.73 Å not included in the table, Mg VII line at 431.29 Å and S XIV line at 445.67 Å have always lower values than the other lines belonging to the same ions. As already noted by Young et al. 1997, this feature is most probably due to some underestimation of the intensity calibration curve around 430-450 Å .
- Cr XIII line at 328.26 disagrees with those of Fe XIII and Si XI, sharing common effective temperature, and are a factor 6 too high.
- Fe XV line at 417.25 Å is stronger than expected and does not agree with the rest of the Fe XV lines. This behavior has already been observed with the ratio method (Young et al. 1997, Feldman 1992, Brosius et al. 1996).
- S XIII and S XIV lines are not consistent with the present ionization balance.

Several other lines deserve a few comments :

- The observed intensities of both the two Cr XIV lines and Cr XIII ($logT_o$ = 6.33) both disagree with those by Fe XIII, Si XI, Fe XV and Fe XVI, and are expected to have intensities around a factor 6 smaller. This feature is most probably due to an underestimation of the adopted abundance of Cr (Feldman et al. 1992). Cr XIII line at 328 shows the greatest discrepancy, but it is blended with a couple of Al VIII lines. Their presence is not able to justify the gap between Cr XIII and the other elements.
- The observed intensities of the Ni XVIII lines are overestimated by a factor 1.5. Nevertheless the presence of only

Table 1. The SERTS-89 intensities for Active Region and Subflare. Wavelengths are in Angstrom, intensities are in erg cm^{-2} s^{-1} sterad^{-1} and T$_{max}$ in K.

λ	$I_{a.r}$	$\sigma_{a.r}$	I$_{sf}$	σ_{sf}	Ion	T$_{max}$
237.351	319.8	114.0	1090.0	370.0	He II	4.7
243.032	532.9	122.2	1290.0	330.0	He II	4.7
303.784	72226.9	20050.0	133000.0	34000.0	He II	4.7
312.429	12.6	10.2	74.8	36.0	C IV	5.0
384.165	8.8	3.6	46.3	13.4	C IV	5.0
419.718	15.0	3.4	19.8	5.8	C IV	5.0
358.455	16.0	5.4	51.7	22.0	Ne V	5.5
359.378	28.0	6.0	85.5	18.9	Ne V	5.5
416.208	21.9	4.8	123.0	16.1	Ne V	5.5
399.837	14.0	3.9	69.2	12.9	Ne VI	5.6
401.139	30.9	5.6	108.0	14.9	Ne VI	5.6
401.936	85.3	13.7	328.0	39.0	Ne VI	5.6
433.161	6.7	4.2	38.6	11.8	Ne VI	5.6
435.632	8.9	3.2	49.0	11.0	Ne VI	5.6
353.084	11.2	5.3	31.8	15.1	Mg V	5.4
355.339	11.9	8.5	37.7	18.0	Mg V	5.4
270.401	60.4	25.0	220.0	117.0	Mg VI	5.6
349.162	62.5	11.9	136.0	29.0	Mg VI	5.6
387.955	9.7	3.7	15.9	6.6	Mg VI	5.6
399.275	9.8	2.6	31.0	11.9	Mg VI	5.6
400.668	18.2	3.5	42.1	9.6	Mg VI	5.6
278.407	129.6	34.3	275.0	130.0	Mg VII	5.8
365.210	27.7	5.9	41.0	13.3	Mg VII	5.8
367.675	54.6	7.7	88.3	19.7	Mg VII	5.8
429.132	12.7	3.5	23.2	8.9	Mg VII	5.8
431.288	20.3	4.7	39.4	11.6	Mg VII	5.8
434.917	31.9	5.4	64.9	11.5	Mg VII	5.8
313.736	84.4	17.7	272.0	71.0	Mg VIII	5.9
315.024	294.1	42.6	537.0	91.0	Mg VIII	5.9
317.008	72.0	17.9	63.5	32.0	Mg VIII	5.9
339.000	65.8	11.5	76.9	22.0	Mg VIII	5.9
430.445	46.8	6.7	85.6	14.1	Mg VIII	5.9
436.726	78.3	10.9	145.0	20.0	Mg VIII	5.9
368.063	1267.7	165.8	2000.0	230.0	Mg IX	6.0
276.850	75.6	24.4	147.0	55.0	Si VIII	5.9
314.345	64.0	14.3	102.0	38.0	Si VIII	5.9
316.220	102.0	17.9	201.0	46.0	Si VIII	5.9
319.839	134.5	19.2	204.0	47.0	Si VIII	5.9
296.137	265.6	44.8	170.0	59.0	Si IX	6.0
344.958	19.8	5.9	40.5	17.9	Si IX	6.0
345.130	88.2	13.5	85.0	24.0	Si IX	6.0
349.872	170.5	22.2	209.0	32.0	Si IX	6.0
258.368	467.6	79.4	466.0	155.0	Si X	6.1
271.992	157.5	34.8	219.0	98.0	Si X	6.1
277.268	132.0	34.6	248.0	87.0	Si X	6.1
347.406	267.8	64.8	176.0	30.0	Si X	6.1
303.324	3609.8	446.9	3900.0	460.0	Si XI	6.2
365.419	48.8	8.1	56.1	17.2	Si XI	6.2
371.499	17.0	5.1	29.5	10.3	Si XI	6.2
256.683	644.1	95.6	760.0	169.0	S XIII	6.4
417.640	203.5	28.8	509.0	59.0	S XIV	6.4
445.660	72.8	10.6	177.0	23.0	S XIV	6.4

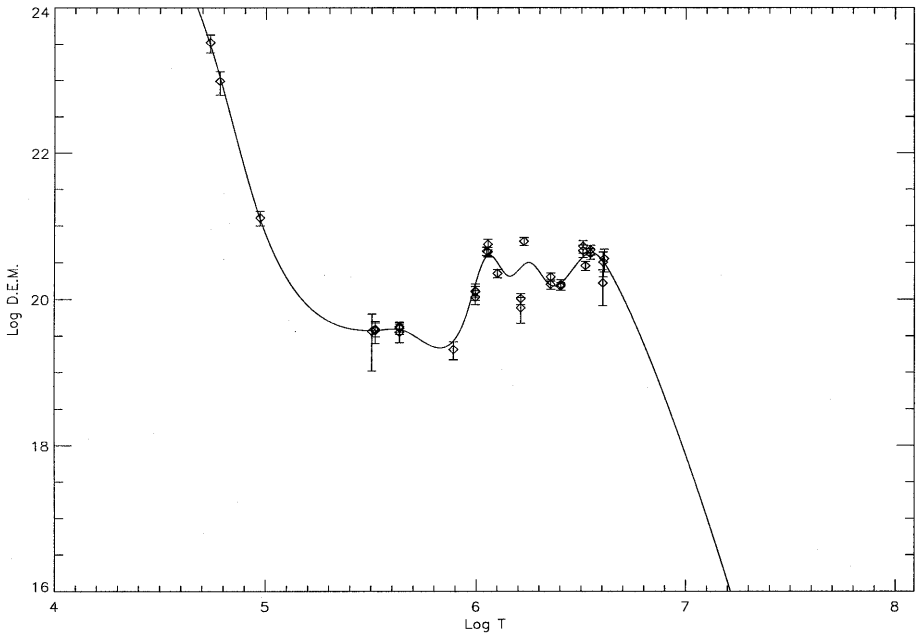

Fig. 4. Differential emission measure for the SERTS-89 averaged Active Region fluxes. Details on the analyzed lines are reported in the text.

one ion makes it difficult to understand if the discrepancy should be attributed to the abundance of Nickel or to the ionization fraction of Ni XVIII.

- Fe XVII 409.71 Å seems to have a lower intensity than the other Fe XVII lines.
- Fe X line at 365.57 Å has a higher intensity than the other Fe X transition. This line is blended with a Ne V transition expected at 365.60 Å which could provide 25 % of the total intensity.
- Cr XIV line at 389.85 Å is higher than expected by the theoretical ratio with the 412.04 Å. No line blending is expected.
- Mg VII line at 278.41 Å is blended with the Si VII transition at 278.44 Å , not reported in the SERTS89 catalogue.
- There seems to be an inconsistency between the observed intensity of the Fe XI and Fe X lines, the former being unexpectedly weaker than the latter. We suggest that this behavior is determined by some problems of the relative ionization equilibrium abundances of the two ions. On the contrary there is fairly good agreement between Fe X and the Mg IX 368.07 Å line which share common $logT_t$ = 6.06.
- There is an huge inconsistency between Fe XIII lines ($logT_t$ = 6.26) and the Be-like Si XI transition 303.23 Å ($logT_t$ = 6.21). The latter line seems to be stronger than expected. It is not clear if the problem is to be found in the atomic transition probabilities of the CHIANTI Si XI model, in those of Fe XIII (see Fe XIII analysis for further details) or in some problems in the abundance of Silicon. It is difficult to understand this behavior since Si XI is the only Silicon ion presenting density insensitive lines. Moreover Si XI line is on the wings of the very strong He II 304. Nevertheless several other Si lines are observed in the present spectrum and they can be used for checking the behavior of Si XI (see the Conclusions).
- There is inconsistency between the observed intensities of Fe XVI ($logT_t$ = 6.50) and S XIV ($logT_t$ = 6.51). This problem may be caused both by relative element abundance problems or by the relative ionization equilibrium abundances of the two ions. Since S XIV is also in conflict with the Be-like S XIII it is not possible to determine which of the problems is the cause of this discrepancy.

3.3. Analysis of the observed intensities

3.3.1. Density insensitive ions

The He II, C IV, Mg V, Ne VI lines show no density dependence and are used just to check the agreement among lines of the same ions. Only lines of NeVI deserve a few comments: the observed spectrum of Ne VI includes 5 fully resolved lines. Lines 399 and 401.9 originate from the same upper level $2s2p^2$-$^2P_{3/2}$, while lines 433 and 435 originate from level $2s2p^2$-$^2S_{1/2}$. All the observed lines do not depend on electron density, so they are expected to have very similar L functions. Nevertheless, as noted in the d.e.m. analysis, while lines 399, 401.1 and 401.9 show an excellent agreement the L functions of lines 433 and 435 are lower than the other by a factor $2.1^{+1}_{-0.5}$. It is worth noting that the 433 and 435 lines have identical (within the uncertainties) L functions, satisfying in this way the requirement for density independent lines.

Since the behavior of 433 and 435 lines is common for the SERTS-89 spectral lines in the range 430-450 Å (see Sect. 3.2), we think that there is a problem in the intensity calibration for this spectral range. It is worth noting that this method allows to estimate the correction factor for the intensities much more easily than the ratio method. The other lines pertaining to the other ions do not present any problem.

Table 2. The SERTS-89 intensities for Active Region and Subflare. Wavelengths are in Angstrom, intensities are in erg cm^{-2} s^{-1} sterad^{-1} and T$_{max}$ in K.

λ	$I_{a.r}$	$\sigma_{a.r}$	I$_{sf}$	σ_{sf}	Ion	T$_{max}$
328.259	115.3	17.6	85.2	33.0	Cr XIII	6.2
389.854	94.3	12.0	114.0	17.0	Cr XIV	6.25
412.039	36.7	5.5	48.8	9.2	Cr XIV	6.25
345.735	92.6	13.3	110.0	24.0	Fe X	6.0
365.565	49.4	8.2	98.1	15.8	Fe X	6.0
308.575	95.5	22.2	209.0	66.0	Fe XI	6.1
341.114	43.6	8.0	76.0	24.0	Fe XI	6.1
352.672	163.0	20.7	141.0	23.0	Fe XI	6.1
358.667	90.9	12.8	79.6	18.6	Fe XI	6.1
369.163	48.3	7.1	31.6	12.7	Fe XI	6.1
195.115	1494.6	291.8	1720.0	800.0	Fe XII	6.1
200.408	425.5	131.8	762.0	280.0	Fe XII	6.1
291.007	136.9	26.6	115.0	57.0	Fe XII	6.1
338.273	91.3	14.2	137.0	33.0	Fe XII	6.1
346.857	84.0	11.8	70.8	24.0	Fe XII	6.1
352.106	177.0	23.1	196.0	30.0	Fe XII	6.1
364.468	291.5	35.2	260.0	35.0	Fe XII	6.1
202.043	827.1	148.6	504.0	250.0	Fe XIII	6.2
203.824	1291.1	216.4	1580.0	430.0	Fe XIII	6.2
221.830	178.6	64.2	301.0	116.0	Fe XIII	6.2
246.195	176.0	67.6	454.0	220.0	Fe XIII	6.2
251.943	443.9	76.7	536.0	220.0	Fe XIII	6.2
312.174	106.1	17.0	111.0	40.0	Fe XIII	6.2
318.120	112.8	19.3	190.0	54.0	Fe XIII	6.2
320.800	216.6	29.9	176.0	40.0	Fe XIII	6.2
348.182	161.5	20.8	127.0	30.0	Fe XIII	6.2
359.644	183.3	22.9	171.0	26.0	Fe XIII	6.2
211.315	1267.9	185.4	1230.0	310.0	Fe XIV	6.3
219.117	517.4	85.8	436.0	139.0	Fe XIV	6.3
220.072	322.1	66.5	218.0	82.0	Fe XIV	6.3
252.201	202.0	82.5	619.0	250.0	Fe XIV	6.3
264.783	1300.1	168.0	1170.0	176.0	Fe XIV	6.3
274.209	1301.5	162.3	1000.0	141.0	Fe XIV	6.3
334.171	809.7	98.7	641.0	80.0	Fe XIV	6.3
353.833	339.8	45.0	601.0	73.0	Fe XIV	6.3
447.343	41.9	5.7	50.2	10.7	Fe XIV	6.3
284.158	9310.8	1150.9	10100.0	1150.0	Fe XV	6.3
321.782	38.2	11.3	109.0	44.0	Fe XV	6.3
327.030	105.3	17.2	145.0	41.0	Fe XV	6.3
372.758	19.2	5.8	30.5	12.9	Fe XV	6.3
417.245	421.2	51.4	411.0	47.0	Fe XV	6.3
251.067	515.2	106.7	969.0	280.0	Fe XVI	6.4
262.978	765.4	110.6	1330.0	193.0	Fe XVI	6.4
335.401	11851.8	2282.9	24800.0	5800.0	Fe XVI	6.4
360.754	4932.0	941.7	10200.0	1640.0	Fe XVI	6.4
347.814	15.4	5.3	46.2	16.0	Fe XVII	6.6
350.477	18.5	6.9	113.0	21.0	Fe XVII	6.6
409.705	5.5	2.8	40.0	9.4	Fe XVII	6.6
291.988	385.9	59.5	1090.0	149.0	Ni XVIII	6.5
320.558	162.6	26.7	484.0	67.0	Ni XVIII	6.5

Table 3. Lines used for the d.e.m. analysis, listed in order of increasing temperature.

Ion	λ (Å)	Ion	λ (Å)
He II	237.35	Fe X	365.57
He II	303.78	Fe XI	352.67
C IV	419.72	Cr XIII	328.26⋆
Ne V	358.46	Si XI	303.32
Ne V	359.38	Fe XIII	246.20
Mg V	353.08⋆	Fe XIII	251.94
Mg V	355.34	Cr XIV	389.85
Ne VI	399.84	Cr XIV	412.04
Ne VI	401.14	Fe XV	284.16
Ne VI	401.94	Fe XV	327.03
Ne VI	433.16⋆	Fe XV	417.25⋆
Ne VI	435.63⋆	S XIII	256.68⋆
Mg VII	278.41⋆	Fe XVI	335.40
Mg VII	429.13	Fe XVI	360.75
Mg VII	431.29⋆	S XIV	417.64
Mg VIII	313.74	S XIV	445.66⋆
Mg VIII	315.02	Fe XVII	347.81
Mg VIII	317.01	Fe XVII	350.48
Mg VIII	339.00	Fe XVII	409.71
Mg VIII	430.45⋆	Ni XVIII	291.99
Mg IX	368.06	Ni XVIII	320.56
Fe X	345.74		

3.3.2. Density sensitive ions

– **Ne V**: The L-functions for Ne V are plotted in Fig 5; for each line the observed flux plus and minus error identifies on the plot a strip of possible L(N_e) solutions for that line, and the area common to all the lines, marked by crosses, identifies the L(N_e) solutions. The observed Ne V spectrum contains 3 lines, two of which (358.455 and 359.378) are originated from the same upper level 2s2p^3-^{3}S$_1$. The L functions of these two lines are expected to be nearly identical. Line 416.208 is density dependent for N$_e$ $\leq$ 10^9 cm^{-3}. None of these lines is blended with unresolved transitions. We note that also the line 365.603 should have been observed, but it is blended with the observed Fe X line at 365.558, as noted during the d.e.m. analysis. The electron density measurement provides unexpectedly a very low value. Unfortunately no other density sensitive lines formed at such low temperatures are available in SERTS 89 spectrum so we are not able to check the consistency of this measure of N_e. The three lines allow to identify a common solution with $24.7 \leq logL \leq 25.0$ and $7.4 \leq logN_e \leq 8.3$; this ion is the coldest one (log T_o = 5.50) among those giving a density evaluation.
– **Mg VI**: Mg VI shows five lines, sufficiently density sensitive for $N_e \leq 10^{10}$ cm^{-3} to provide a density diagnostic. The L functions of lines 399.275 and 400.668 perfectly agree but do not supply any density measurements since they originate from two levels of the same multiplet whose population depends on N_e in the same way. The other lines don't agree among each other. The behavior of line 270.4 is uncertain

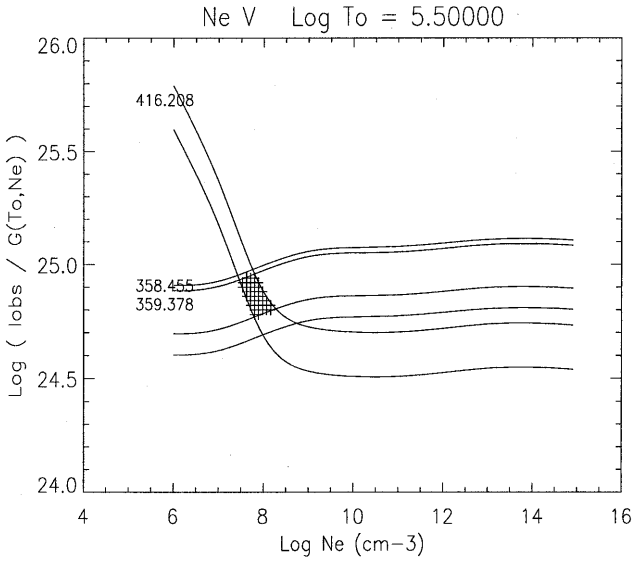

Fig. 5. The ratio of the observed intensity to the $G(N_e, T_o)$ is plotted versus the logarithmic density for all the lines of Ne V. For each line the observed intensity plus and minus the error is considered.

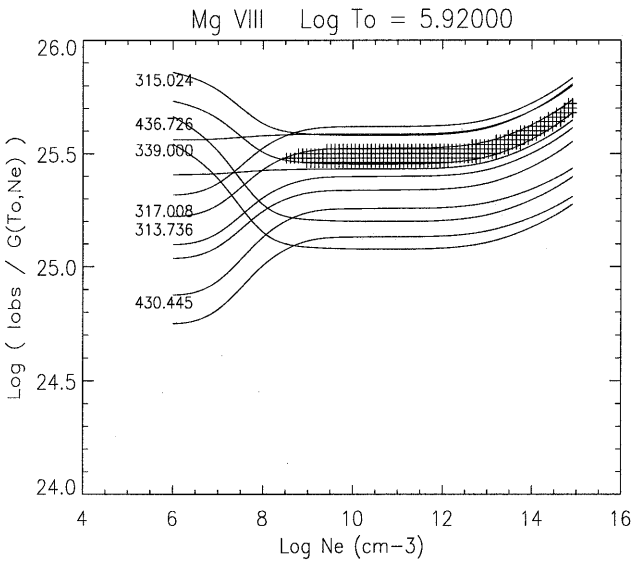

Fig. 6. The ratio of the observed intensity to the $G(N_e, T_o)$ is plotted versus the logarithmic density for all the lines of Mg VIII. For each line the observed intensity plus and minus the error is considered.

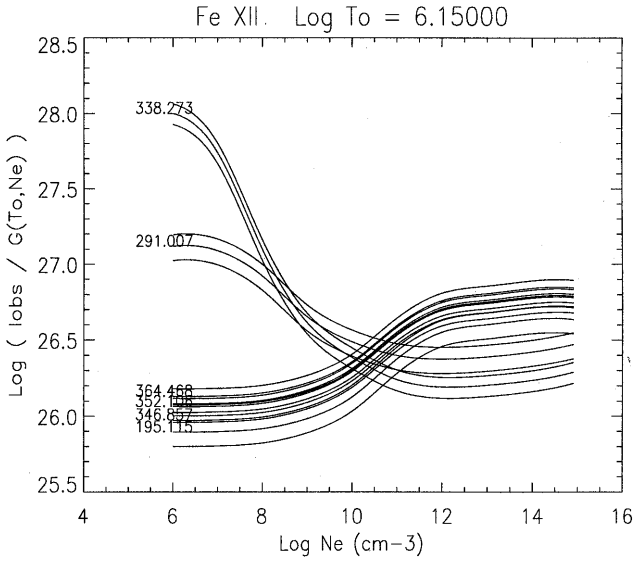

Fig. 7. Results of the method for Fe XII. See comments in the text

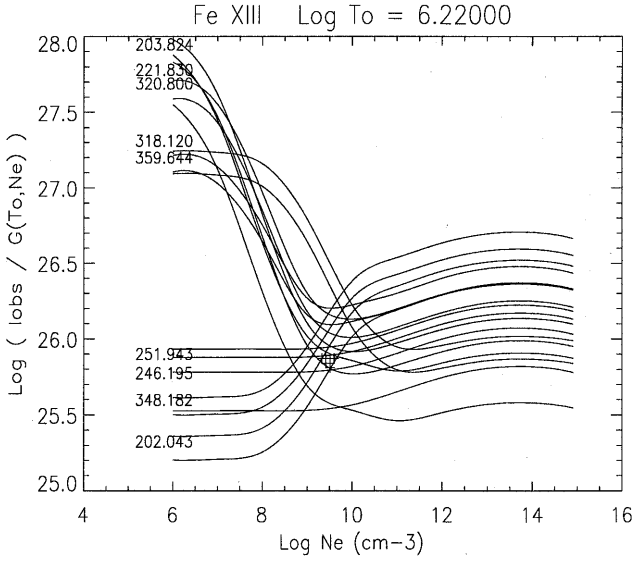

Fig. 8. Results of the method for Fe XIII. See comments in the text

since no unresolved contributions are expected and probably the problems are to be found in the atomic calculations.

– **Mg VII**: Six lines of Mg VII have been observed; a very narrow interval of solutions is common to all the lines except 278.407. However, a small correction of line 434.917 (about 1.5 larger) allows any log density value larger than 7.6. Line 278.407 has higher L values than the rest of the lines by a factor 3. This difference is far greater than the experimental uncertainties and is most probably due to the unresolved contribution of Si VII 278.443 line. From the comparison of the L functions we are able to evaluate the expected contribution of the Mg VII line to be around 43.2 erg cm^{-2}s^{-1}sterad^{-1} while the Si VII transition intensity should be 86.4 erg cm^{-2}s^{-1}sterad^{-1}. Unfortunately no averaged Active Region intensity for any Si VII line has been reported (see tables 2 and 3) and it is not possible to check directly this conclusion.

– **Mg VIII**: For Mg VIII (Fig. 6) lines 436.726 and 430.445 do not agree with the others that identify a common region $logN_e \geq 8.4$ and $25.6 \leq LogL \leq 25.8$. The L functions of the two lines are in good agreement with each other but have values lower by a factor 2 than those of the L functions of the other lines. This feature, already outlined by the Ne

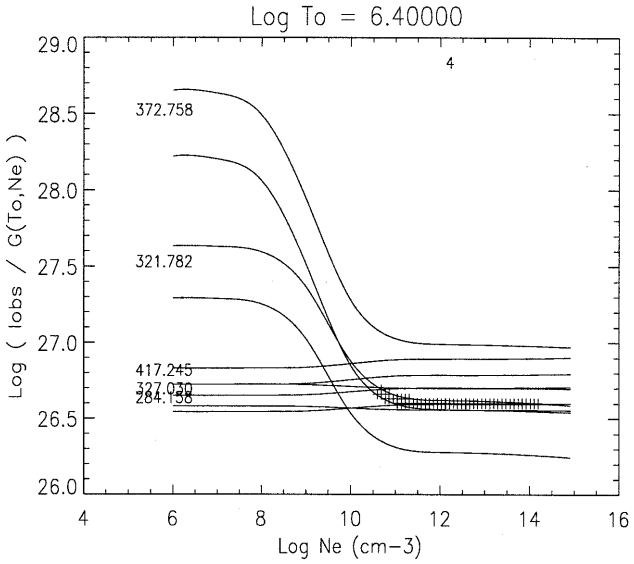

Fig. 9. Results of the method for Fe XV. See comments in the text

VI and Mg VII transitions in the same wavelength region, is probably due to intensity calibration problems.

- **Si VIII**: Si VIII lines 314.345, 316.220 and 319.839 overlap and the intersection with 276.85 allows a common solution for $10 \leq logN_e \leq 11.6$ and $25.4 \leq logL \leq 25.7$.
- **Si IX**: Si IX allows the evaluation of only a lower limit $logN_e \geq 9.2$. Line 296.137 only very marginally agrees with the others, showing a too strong observed intensity. The reason for this behavior is probably due to an unresolved blending contribution.
- **Si X**: Si X (Fig. 1) shows one of the best results; there are 5 density dependent lines which allow density diagnostic. Line 356 is a blend of two Si X transitions. The lines 271 and 277 originate from the same upper level and their L functions are nearly identical, as expected from theory. All the L functions meet for densities in the range $10^{8.6}$-$10^{9.8}$ cm^{-3}.
- **Si XI** Also the three Si XI lines agree over a rather narrow range of solutions: $10^{8.8}$-$10^{9.4}$ cm^{-3}. The L functions for these transitions have values $LogL = 26.64 \pm 0.07$. The values of the L function are higher than those found with Fe XIII, which shares the same log T_o, while the value of the electron density is consistent with that provided by this ion.

A large number of highly ionized iron lines have been detected in the SERTS 89 observation and they provide a wealth of strong emission lines extremely useful for density diagnostic.

- **Fe X**: The two Fe X lines are almost density independent; they agree reasonably within the experimental uncertainties but do not give any density diagnostic.
- **Fe XI** Two pairs of Fe XI lines originate from the same upper level: 352.672 and 369.163 decay from the 3s3p^5-^{3}P$_2$ level and their L functions completely overlap, while 358.667 is totally incompatible with 341.114 which decays from the same upper level 3s3p^5-^{3}P$_1$ and shares common solutions with the other pair. The disagreement is probably due to unresolved contributions from lines belonging to Si XI, Ne IV and Ne VI to the Fe XI line 358.667. Line 308.575 allows to find solutions for any $logN_e \geq 10.6$.
- **Fe XII**: The Fe XII Active Region spectrum shows 7 lines density sensitive in the range 10^8-10^{12} cm^{-3} (Fig. 7). The L functions of 6 lines meet for densities in the range $10^{9.9}$-$10^{10.6}$ cm^{-3} within the limits of their error bars. Line 291 seems to have a slightly high observed intensity but no contributions from other Fe XII line or other ions' lines are expected. Line 195 has a too low L function. A problem arises with line 200, not shown in Fig. 7, because its L function is a factor 10 greater than all the others and no contributions from other lines are expected. This line is a second order lines but since no other second order lines (like Fe XII 195) suffer from a too high L function we do not expect to have any intensity calibration uncertainties. The behavior of this line is not understood.
- **Fe XIII**: Several observed lines of Fe XIII are strongly density dependent in the density range 10^8-10^{11} cm^{-3}, and most of them meet for densities between $10^{9.3}$ and $10^{9.6}$ cm^{-3} (Fig. 8). Nevertheless the Active Region spectrum of Fe XIII presents a very strange feature: there is not good agreement between the lines with wavelength shorter than 300 Å and those with wavelength longer than 300 Å. For instance lines 202 and 348 never meet and lines 203, 221 cross lines 318, 320 and 359 for densities much lower than those found with other lines. If we plot all the L functions of lines longward 300 Å in a separate figure we see that the agreement between these lines is very good and the determination of the electron density of the emitting source much less controversial. The same behavior is found for lines shortward than 300 Å and it is important to notice that the values of electron density measured with this two sets of lines are consistent: $10^{9.35}$-$10^{9.75}$ for lines with $\lambda \leq 300$ Å , $10^{9.1}$-$10^{9.6}$ for $\lambda \geq 300$ Å. The values of the L functions at the crossing point instead are different: lines longward 300 Å have L functions higher than the others by a factor $\simeq 2.3$. One could think to a systematic effect on the experimental intensity calibration: this feature should be plainly visible also for all the observed lines but all the other ions do not show this behavior. We think that the explanation of this behavior is to be found in the atomic physics calculations that provide the adopted collisional and radiative transition rates. The only thing to be noted about single lines is that the observed intensity of line 318 appears to be stronger than the other 300 Å lines by a factor 1.4; it is worth noting that a similar behavior of line 318 is seen in nearly all CDS NIS-1 spectra (P.R. Young, private communications).
- **Fe XIV**: There are 9 observed Fe XIV lines which are density sensitive in the range 10^8-10^{11} cm^{-3} and can potentially give density diagnostic. Nevertheless the behavior of the Fe XIV is quite complex. Lines with wavelength shorter than 260 Å are consistent with each other and their L functions cross in the density range $10^{9.3}$-$10^{9.6}$ cm^{-3}. All the other lines do not cross this meeting point and have a greater L function

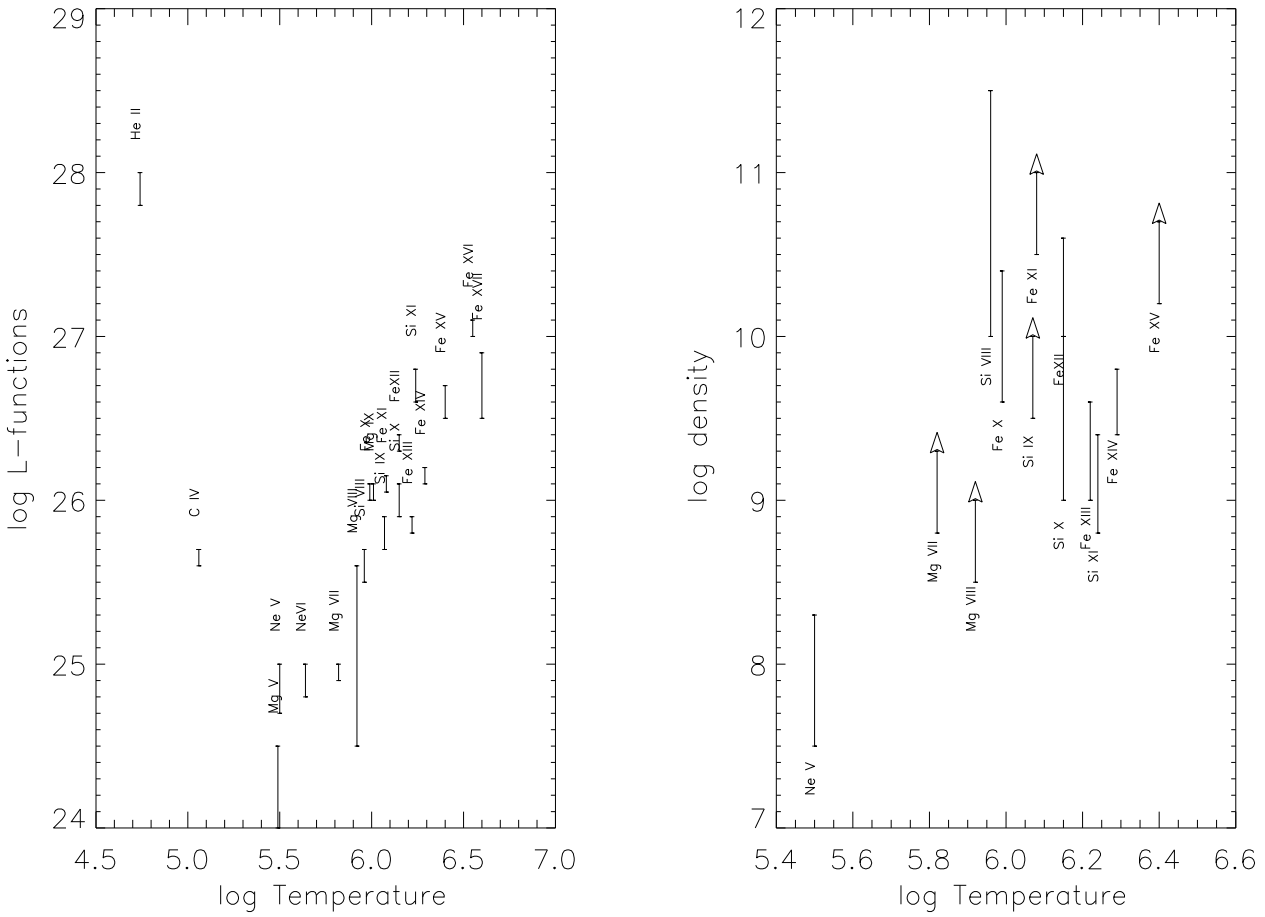

Fig. 10. a (left) The L-functions versus temperature solutions for each ion. **b** (right) The density versus temperature solutions

than expected. The two lines 252 and 264 originate from the same upper level but their L functions agree only at the limit of their error bars, lines 334.2 and 353.8 meet for densities in the range $10^{9.5}$-$10^{9.9}$ cm^{-3} but the values of the L functions in that point is greater than the one provided by the lines with $\lambda \leq 260$ Å by a factor 2.5. The intercombination line at 447 has L values even higher. It is not easy understand the reason for this behavior, since there are not unresolved contributions for all these lines and the problem is most likely to be found in the theoretical data used for calculating the $Contribution Functions$ of these lines.

– **Fe XV**: The electron densities greater than $10^{10.2}$ cm^{-3} satisfy four Fe XV lines out of five. Line 417.245 is only marginally too high.
– **Fe XVI**: Fe XVI presents perfectly overlapping four L-functions with no density diagnostic, as expected.

4. Conclusions

The results of the above discussion are summarized in Fig. 10.

In Fig. 10a, the L-function resulting from the analysis of both density sensitive and density insensitive ions of Sect. 3 is plotted versus the effective temperature for each ion. The L-function is directly related to the d.e.m. as shown in Sect. 2.

All Si ions but SiXI are lower about twice then the Fe lines at the same temperature; this could suggest that the adopted silicon abundance is too high.

In Fig. 10 b, the density is plotted versus the effective temperature. For several ions only lower limits are put by the observations. No definite suggestion occurs either in favor of constant density or of constant pressure hypothesis.

Neither a constant density or a constant pressure solution can satisfy all the data; in particular the electron density provided by Ne V is very small, though it is necessary to remind that the Ne V value is due to only one line and that there are no other lines formed at similar temperatures that can provide a density diagnostic. Of further interest is the fact that also Fe XII and Si X give different measurements of electron density though their temperatures T_o and T_{max} are very similar.

Another important result is given by the systematic low intensity of lines whose wavelength is around 430 Å , as seen in Ne VI, Mg VII, Mg VIII and S XIV which causes the L functions of these transitions to be lower than all the other of the same ion. The suggested correction factor is around 2. Of further interest is the fact that we found evidence for prob-

lems on both element abundance and ionization equilibrium for Chromium, moreover also S XIII and S XIV do not agree with each other, while Ni XVIII needs a correction of a factor 1.5 to the $ContributionFunction$ of both the observed lines. It is not possible to understand if this correction is due to element abundance or ionization equilibrium problems.

Using the d.e.m. it is also possible to calculate a synthetic spectrum and compare the results with all the observed intensities. The most important conclusions have been confirmed by this procedure: in particular the Silicon abundance adopted in the calculation of the synthetic spectrum (Feldman et al. 1992) is higher than observations indicate by a factor around 3, and there is a discrepancy between the adopted ion abundances of Si VIII, IX, X and the Si XI one.

To summarize the results, we note that the method described in this paper supplies detailed information for:

- model temperature and density of the source along the line of sight
- verify the chemical composition assumed to compare observations and theory
- check the ionization equilibrium values for each ion
- verify the intensity calibration at different wavelength
- suggest incorrect line identifications and blending
- select lines where atomic physics needs to be improved

Acknowledgements. We warmly thank R. Thomas and J. Brosius for having kindly supplied the SERTS89 data for active region and subflare and to have allowed their use for this method testing.

References

Arnaud,M. and Rothenflug,R. 1985, A&AS, 60, 425
Arnaud,M. and Raymond,J.C. 1992, ApJ, 398, 394
Brosius, J.W., Davila, J.M., Thomas, R.J., Monsignori Fossi, B.C., 1996, ApJS, 106, 143
Dere,K.P., Landi,E., Mason,H.E., Monsignori Fossi,B.C. and Young,P.R. 1996, A&A in press
Doschek G.A., 1990, ApJS, 73,117
Dwivedi, B.N., 1994, Sp. Sc. Rev., 65,289-316
Feldman, U., 1992, ApJ, 385, 758
Feldman, U., Mandelbaum P., Seely J.L., Doschek G.A., Gursky H., 1992, ApJS, 81, 387
Harrison, R.A. and Thompson, A.M. (eds.), 1992, *Intensity integral inversion techniques: a study in preparation for the SOHO mission*, RAL-91-092, Rutherford Appleton Laboratory.
Jordan, C., 1969, MNRAS, 142, 501
Mason,H. E.,1991,Adv. Sp.Res.11,(1),293-301
Mason, H.E.and Monsignori Fossi, B.C.,1994, The Astron. Astrophys. Rev., 6,123
Thomas, R.J., and Neupert, W.M., 1994, ApJS, 91, 461
Young,P.R., Landi,E. and Thomas, R.J., 1997, A&A submitted.

This article was processed by the author using Springer-Verlag LaTeX A&A style file *L-AA* version 3.